Article

PyrPeg, a Blood-Brain Barrier-Penetrating Two-Photon Imaging Probe, Selectively Detects Neuritic Plaques, not Tau Aggregates

Ji-Woo Choi, Yeon Ha Ju, Yunsook Choi, Seung Jae Hyeon, Changdev G. Gadhe, Jong-Hyun Park, Mun Seok Kim, Seungyeop Baek, YoungSoo Kim, Ki Duk Park, Ae Nim Pae, Hoon Ryu, C. Justin Lee, and Bong Rae Cho

Just Accepted

PyrPeg, a Blood-Brain Barrier-Penetrating Two-Photon Imaging Probe, Selectively Detects Neuritic Plaques, not Tau Aggregates

Ji-Woo Choi,[†,◇] Yeon Ha Ju,[‡,§,◇] Yunsook Choi,[‖,⊥] Seung Jae Hyeon,[#] Changdev G. Gadhe,[▽]

Jong-Hyun Park,[▽] Mun Seok Kim,[○] Seungyeop Baek,[¶] YoungSoo Kim,[¶] Ki Duk Park,[▽,◆] Ae Nim

Pae,[▽,◆] Hoon Ryu,[#,■] C. Justin Lee,*[,‡,§] and Bong Rae Cho*[,†,○,]

[†] KU-KIST Graduate School of Converging Science and Technology, Korea University, 145 Anam-ro, Seongbuk-gu, Seoul, 02841, Republic of Korea

[‡] Center for Cognition and Sociality, Institute for Basic Science (IBS), 55 Expo-ro, Yuseong-gu, Daejeon, 34126, Republic of Korea

[§] IBS School, University of Science and Technology, 217 Gajeong-ro, Yuseong-gu, Daejeon, 34113, Republic of Korea

[‖] Center for Functional Connectomics, Korea Institute of Science and Technology (KIST), 5 Hwarangro 14-gil, Seongbuk-gu, Seoul, 02792, Republic of Korea

[⊥] Department of Cellular and Molecular Physiology, Yale University School of Medicine, New Haven, CT 06511, USA

[#] Centers for Neuromedicine and Neuroscience, Brain Science Institute, KIST, 5 Hwarangro 14-gil, Seongbuk-gu, Seoul, 02792, Republic of Korea

[▽] Convergence Research Center for Diagnosis, Treatment and Care System of Dementia, KIST, 5 Hwarangro 14-gil, Seongbuk-gu, Seoul, 02792, Republic of Korea

[○] Department of Chemistry, Daejin University, 1007 Hoguk-ro, Pocheon-si, Gyeonggi-do, 11159, Republic of Korea

[¶] Integrated Science and Engineering Division, Department of Pharmacy and Department of Biotechnology, and Yonsei Institute of Pharmaceutical Sciences, Yonsei University, 85 Songdogwahak-ro, Yeonsu-gu, Incheon, 21983, Republic of Korea

[◆] KHU-KIST Department of Converging Science and Technology, Kyung Hee University, Seoul, 02447, Republic of Korea

[■] Boston University Alzheimer's Disease Center (BU ADC) and Departments of Neurology, Boston University School of Medicine, Boston, MA 02118, USA

Department of Chemistry, Korea University, 145 Anam-ro, Seongbuk-gu, Seoul, 02841, Republic of Korea

ABSTRACT: Amyloid-β (Aβ) tracers have made a significant contribution to the treatment of Alzheimer's disease (AD) by allowing a definitive diagnosis in living patients. Unfortunately, they also detect tau and other protein aggregates that compromise test accuracy. In AD research, there has been a growing need for *in vivo* Aβ imaging by two-photon microscopy, which enables deep-brain-fluorescence imaging. There is no suitable neuritic Aβ probe for two-photon microscopy. Here we report PyrPeg, a novel two-photon fluorescent probe that can selectively target insoluble Aβ rather than tau and α-synuclein aggregates in the AD model brain and post-mortem brain. When injected intravenously, PyrPeg detects the neuritic plaques in the brain and olfactory bulb of the AD model. PyrPeg may serve as a useful blood-brain-barrier-penetrating diagnostic tool for optical and functional monitoring of insoluble forms of Aβ aggregates in the living AD brain.

INTRODUCTION

The diagnosis of Alzheimer's disease (AD) is based on the detection of amyloid-β (Aβ) misfolding in the brain, tau

abnormalities, and neurodegeneration.[1] The accumulation of Aβ plaques is the earliest key event in AD progression, beginning at the asymptomatic stage of AD, and is considered a biomarker of disease onset. Aβ plaques are classified as diffuse and neuritic plaques. Diffuse plaques are non-neuritic, not associated with glial activation, and thus not regarded as pathological biomarkers.[2,3] By contrast, neuritic plaques, also known as senile plaques, are extracellular deposits of Aβ, surrounded by abundant activated microglia and astrocytes and associated with synaptic loss and cognitive impairment.[4] Therefore, evaluation of neuritic plaques can be useful for the diagnosis of AD. Up to now, it has been possible to visualize neuritic plaques by immunostaining in fixed tissues. Nevertheless, currently, there is no available optical Aβ probe that specifically labels neuritic plaques *in vivo*.

Optical imaging with fluorescent probes is a rapid and inexpensive screening method for AD. So far, many optical imaging probes for Aβ have been developed, such as Congo red, thioflavin-S (Th-S), and A11.[5] Nevertheless, the use of these probes with one-photon microscopy (OPM) requires a short excitation wavelength (<500 nm), which limits the applications for *in vivo* imaging because of the shallow penetration depth (<80 μm), autofluorescence, photobleaching, and phototoxicity.[6] Furthermore, many near-infrared (NIR) probes have been developed, e.g., NIAD-4, CRANAD-2, BAP-1, and 1,4-bis(4′-hydroxystyryl)-2-methoxybenzene (MeO-X04).[7] Although NIR microscopy exploits NIR excitation wavelengths (>700 nm), it is more useful for large objects, such as whole mice, than for micron-sized objects such as cells and tissue slices because of poorer resolution relative to OPM.[8] A practical approach for overcoming these shortcomings is two-photon microscopy (TPM). TPM, which employs two NIR photons for excitation, can detect biological targets deep inside a probe-labeled tissue (>100 μm) for an extended period with intrinsically localized emission and minimum autofluorescence and photodamage artifacts.[6] In addition, three-dimensional (3D) distribution of the targets can be mapped by combining the sectional images.

Recently, a few two-photon (TP) probes for Aβ have been developed, and their utility for *ex vivo* and *in vivo* imaging has been evaluated by TPM.[6,9,10] Among these, QAD1 and SAD1 have dissociation constants (K_d) of 16.2 and 17 nM,[11] respectively. On the contrary, QAD1 and SAD1 are not suitable as AD diagnostic tools because they detect Aβ at 16 nM, which is much lower than the critical aggregation concentration (CAC, 90 nM),[12] thus making it difficult to distinguish the Aβ monomer from the Aβ oligomer. Besides, there is another Aβ probe called "Aβ probe 5," which has a more reasonable K_d value (44.6 nM).[6] Nonetheless, this probe is not suitable for TPM imaging because the TP action cross-section (Φδ), a measure of TP excited fluorescence (TPEF) brightness, is too small (4 GM, where GM = 10^{-50} cm⁴s/photon) to obtain bright TPM images using the laser power (lower than 5 mW at the focal point) that does not cause damage to the cells and tissues.[13] Among the NIR probes, MeO-X04 has Φδ of 75 GM at 720

nm and has been applied to obtain TPM images of a mouse brain slice.[11] On the contrary, this probe has an inhibition constant (K_i = 26. 8 nM) less than CAC and can detect tangles and cerebrovascular amyloids in addition to the Aβ peptides.

Therefore, so far, there is not a suitable TP probe for Aβ peptides, and our aim in this study was to develop and test such a probe. Here, we designed and developed PyrPeg: a combination of a pyrazine derivative, which is an efficient fluorophore, and polyethylene glycol, which is a hydrophilic chain. This design is based on a previously described Pyr-affibody (a TP probe for HER2 [human epidermal growth factor receptor 2]), which has been reported to emit strong TPEF for the detection of breast cancer cells in a xenograft model using TPM.[14] We describe the design, chemical synthesis, photophysical and biochemical properties, and biological activities of PyrPeg. Because PyrPeg is a small planar uncharged molecule (<500 Da), we anticipated that it would stain tissue, possibly cross the blood–brain barrier (BBB), intercalate into the hydrophobic grooves in the β-sheet structure of Aβ peptides, and emit strong TPEF, thereby allowing the *in vivo* diagnosis of AD. We studied the photophysical properties, binding affinity for Aβ peptides, and selectivity over other proteins and conducted *ex vivo* and *in vivo* imaging experiments with PyrPeg. We also compared the photophysical properties of PyrPeg with those of existing TP probes and its Aβ-detecting abilities with those of Th-S, MeO-X04, and an anti-Aβ antibody. Furthermore, we examined PyrPeg fluorescence in postmortem AD patients' brain sections. Finally, we investigated the fluorescence of PyrPeg in tail-injected transgenic mice (a model of AD) in the olfactory bulb *in vivo* by TPM.

RESULTS AND DISCUSSION

Synthesis and Photophysical Properties. PyrPeg was synthesized in five steps (Figure 1a–e) starting from 3-methoxy-N-methylaniline (compound **2**, Figure 1a).[15] At step a, nosylation of **2** afforded compound **3** in a 77% yield. At step b, demethylation of **3** using BBr3 produced **4** in a 95% yield. At step c, the formylation reaction of **4** produced **5**[16] in a 52% yield. At step d, **5** was then reacted with **1** to obtain **6** in a 42% yield. At step e, PyrPeg was generated in a 53% yield by the deprotection of the nosyl group (Figure 1a, see Supporting Information for details). The solubility of PyrPeg in phosphate-buffered saline (PBS) was found to be 1.0 μM (Figures S2a,b) as measured by the maximum intersection point in a plot of absorbance vs. probe concentration (Figure S2).

PyrPeg showed a maximum absorption wavelength (λ_{max}) of 441 nm with a molar absorption coefficient, ε, of 78,800 cm⁻¹M⁻¹ and a maximum emission wavelength (λ_{fl}) of 525 nm with a fluorescence quantum yield, Φ, of 0.84 in 1,4-dioxane. The λ_{fl} value showed a gradual red shift with a concomitant decrease in Φ as the solvent was changed to a more hydrophilic one (Table 1 and Figure S1). In EtOH, λ_{max} and λ_{fl} appeared at 447 nm (ε = 56,700 cm⁻¹M⁻¹) and 629 nm (Φ = 0.03), respectively, and a large Stokes shift ($\Delta\bar{\nu}$ =
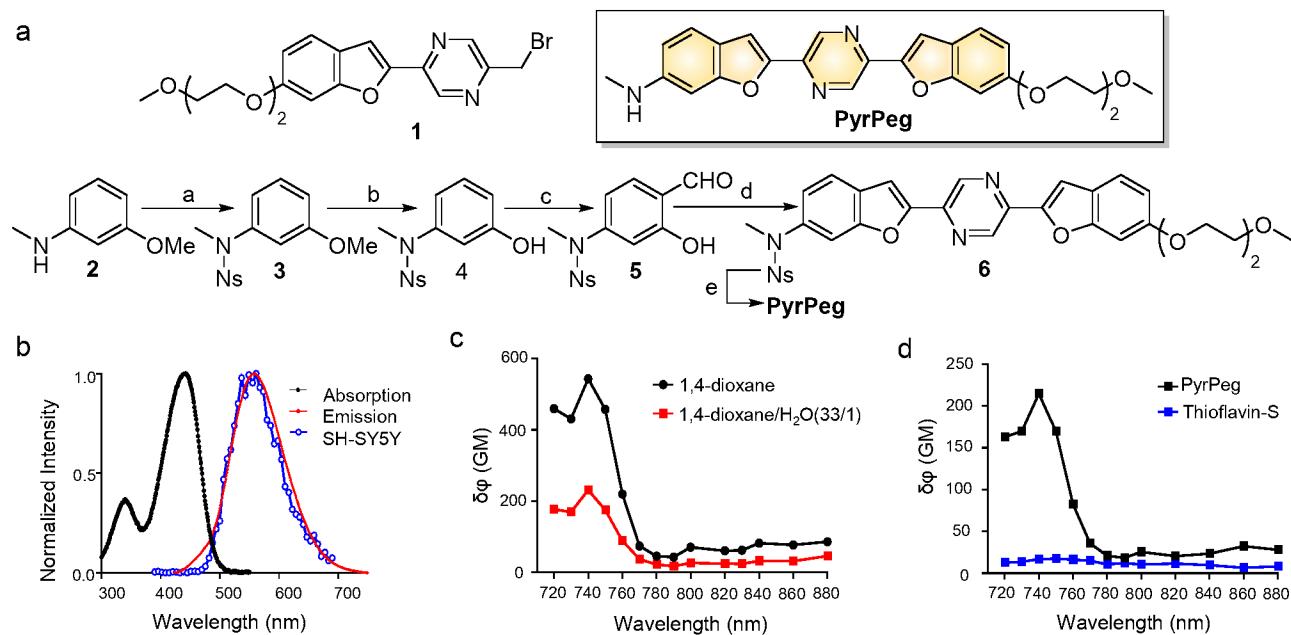
Figure 1. Synthesis and photophysical properties of PyrPeg. (a) Structure and the synthesis of PyrPeg. a) 2-Nitrobenzenesulfonyl chloride, Et_3N, CH_2Cl_2, 0 °C; b) BBr_3, CH_2Cl_2, −78 °C; c) p-paraformaldehyde, $MgCl_2$, Et_3N, CH_3CN, reflux; d) compound **1**, K_2CO_3, dimethylformamide, 100 °C; e) PhSH, K_2CO_3, dimethylformamide, 0 °C. (b) Normalized one-photon absorption (black dots) and emission (red dots) spectra of PyrPeg (1 μM) in 1,4-dioxane–H_2O (33:1) and a two-photon excited spectrum of PyrPeg-labeled SH-SY5Y cells (open blue dots). (c) Two-photon excitation spectra of PyrPeg (1 μM) in 1,4-dioxane (black circles) and 1,4-dioxane–H_2O (red circles). (d) Two-photon excitation spectra of PyrPeg (1 μM, black squares) and Th-S (1 μM, blue squares) in EtOH.

6.5×10^3 cm⁻¹) was noted (Table 1). The solvatochromic shift ($\Delta\lambda_{fl}$) for the switch from 1,4-dioxane to EtOH was 104 nm (Table 1 and Figure S1b). In PBS (pH 7.4), PyrPeg manifested λ_{max} at 422 nm ($\varepsilon = 26{,}430$ cm⁻¹M⁻¹), and its fluorescence was too weak to measure λ_{fl} and Φ accurately (Table 1). PyrPeg emitted broad TPEF in the range of 450–650 nm with λ_{fl} at 560 nm in SH-SY5Y cells (Figure 1b) when excited at 740 nm in scanning lambda mode.

Table 1. Spectroscopic properties of PyrPeg

Solvent (E_T^N)[a]	$\lambda_{max}/\lambda_{fl}$[b]	Φ[c]	$\Phi\delta_{max}$[d]	δ_{max}[e]
Dioxane (0.164)	441[f]/525	0.84	543	650
Dioxane–H_2O, 33:1	440[f]/560	0.34	230	680
EtOH (0.654)	447[f]/629[g]	0.17	-	-
PBS (1.00)	422[f]/-	0.03	-	-
SH-SY5Y cells	-/560[h]	-	1520[i]	-

[a]The numbers in parentheses are normalized empirical parameters of solvent polarity.[17] [b]One-photon absorption and emission maxima except when noted otherwise. [c]Fluorescence quantum yield. The uncertainty was set to ±15%. [d]TP action cross-section (in GM, ±15%). [e]TP cross-section (in GM, ±15%). [f]Molar absorption coefficients (ε) measured in 1,4-dioxane, 1,4-dioxane–H_2O (33:1), EtOH, and PBS are 78,800, 70,850, 56,700, and 26,430 cm⁻¹M⁻¹, respectively. [g]λ_{fl} Stokes shift calculated from λ_{max}, and λ_{fl} in EtOH was 6.5×10^3 cm⁻¹. [h]λ_{fl} of TPEF spectra. [i]Effective TP action cross-section values ($\Phi\delta_{eff}$) measured in SH-SY5Y cells.

The spectrum was broader, and λ_{fl} was blue-shifted by 69 nm, as compared to those measured in EtOH, indicating that the intracellular environment around the probe was more heterogeneous and more hydrophobic than that in EtOH. On the contrary, λ_{fl} is identical to that measured in 1,4-dioxane–H_2O (33:1) (Table 1 and Figure S1b), meaning that this mixed solvent adequately represents the probe's intracellular environment. Therefore, we chose 450–650 nm as the detection window for the bioimaging experiments and 1,4-dioxane–H_2O (33:1) as the model solvent. $\Phi\delta$ of PyrPeg was measured by the fluorescence method.[18] Here, $\Phi\delta$ is the ratio of TP excited photons to photons emitted through fluorescence, and this parameter is a direct measure of brightness.

The maximum $\Phi\delta$ values ($\Phi\delta_{max}$) of PyrPeg in solvents 1,4-dioxane and 1,4-dioxane–H_2O (33:1) were 543 and 230 GM at 740 nm, respectively (Figure 1c and Table 1). The δ_{max} values of PyrPeg, which were calculated by dividing $\Phi\delta_{max}$ by Φ, are 650 and 680 GM in 1,4-dioxane and 1,4-dioxane–H_2O (33:1), respectively (Table 1). $\Phi\delta_{max}$ of PyrPeg is similar to those of PLT-yellow, PMT-yellow, and Pyr-CT, thereby confirming the reliability of $\Phi\delta$ in many derivatives of PyrPeg.[14,19]

Selectivity of PyrPeg for the Oligomer of the Human Amyloid-β42 Peptide ($A\beta_{42}$). To investigate the selectivity of PyrPeg for various amyloidogenic proteins, we treated primary-culture astrocytes with $A\beta_{42}$ fibrils, tau 441 (tau), or α-synuclein (α-syn) for 24 h. We used newly synthesized $A\beta_{42}$[20] and commercially available tau and α-syn. The OPM images of the $A\beta_{42}$-treated cells colabeled with PyrPeg and an anti-Aβ antibody colocalized well, with
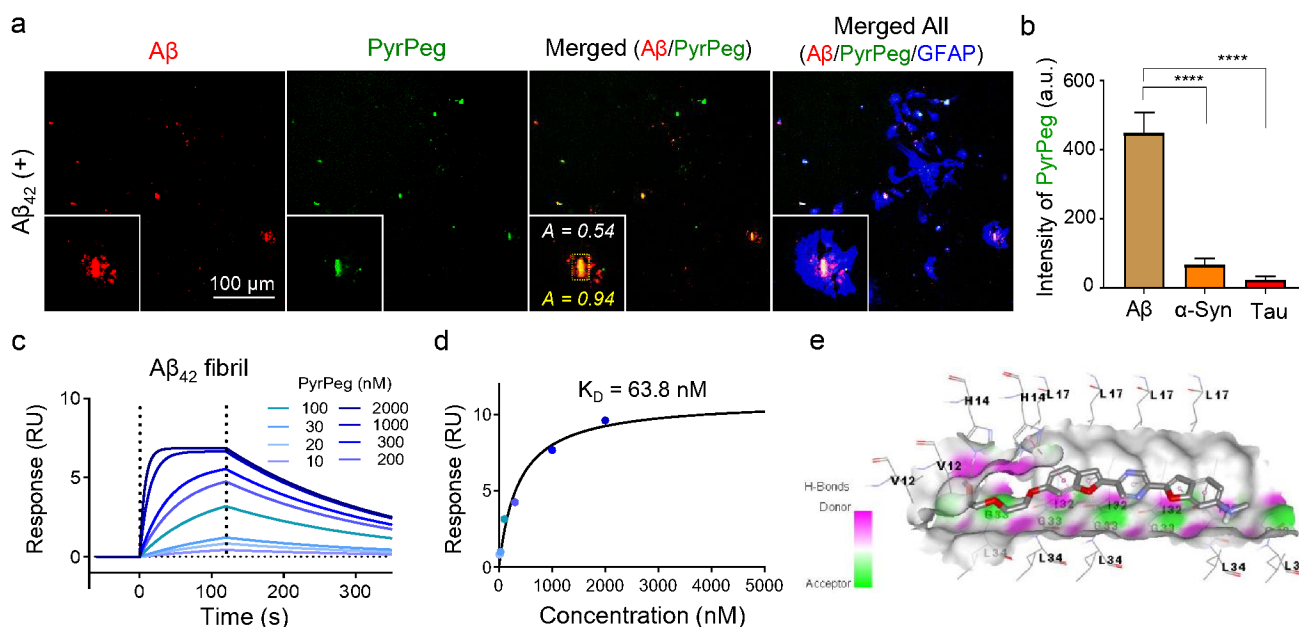
Figure 2. Selectivity of PyrPeg for amyloidogenic proteins. (a) OPM images of astrocytes colabeled with an anti-Aβ antibody, PyrPeg, and GFAP and merged images (the OPM image of GFAP-labeled cells is omitted for simplicity). The cells were pretreated with Aβ$_{42}$ fibrils for 1 day. (b) Relative fluorescence intensities of PyrPeg in the PyrPeg-labeled astrocytes pretreated with Aβ$_{42}$ fibrils, α-syn, or tau 441 for 1 day (see Figure S3 for the OPM images of α-syn– and tau 441-treated cells). ****$P < 0.0001$, one-way ANOVA with Tukey's multiple-comparison test. (c,d) SPR sensorgrams (c) and binding curves for the binding of PyrPeg to Aβ$_{42}$ fibrils (d). Blue dots are the experimental data, and black curves are the fitted curves obtained by means of the BIAcore evaluation software. (e) Molecular docking analysis of PyrPeg inside human Aβ$_{42}$ (glide docking scores for PyrPeg = −8.94 kcal/mol).

the Pearson's colocalization coefficients (A)[21] of 0.54 in the Figure 2a inset and 0.94 in the white square (Figure 2a). This outcome indicates that PyrPeg labels the core of Aβ$_{42}$ (Figure 2a). In sharp contrast, the α-syn– and tau 441-treated cells colabeled either with PyrPeg and α–syn or with PyrPeg and tau 441 showed no overlap, with the A value of 0.00 (Figure S3).

Moreover, the fluorescence intensity of PyrPeg in Aβ$_{42}$-treated astrocytes was much higher than these intensities in α-syn– and tau 441-treated cells (Figure 2b), as confirmed in Aβ$_{42}$-treated SH-SY5Y cells by TPM (Figure S4). These results confirm that PyrPeg is specific for Aβ$_{42}$ fibrils over other amyloidogenic proteins. To quantitatively measure the binding affinity of PyrPeg for Aβ$_{42}$ fibrils and monomers, we obtained surface plasmon resonance (SPR) sensorgrams (Figures 2c and S5a). We employed 10–2000 and 10–5000 nM PyrPeg for the binding assays of fibrils and monomers (Figures 2c and S5b), respectively, because no response was detected when the PyrPeg concentration was lower than 10 nM (Figure S5c,d). The association (k_a) and dissociation rate (k_d) constants and K_d were estimated using the BIAcore evaluation software by fitting the binding curves to a simple bimolecular binding algorithm (Figures 2d and S5b). The K_d values for the binding of PyrPeg to the Aβ$_{42}$ fibrils and monomer were 63.8 and 799 nM, respectively. Thus, the affinity of PyrPeg for Aβ$_{42}$ fibrils is ~12-fold stronger than that for the Aβ$_{42}$ monomer.

Other conventional TP probes, such as QAD1 (16 nM), SAD1 (17 nM), Aβ probe 5 (44.6 nM), PIB (41 nM), and MeO-X04 (26. 8 nM) have K_d (or K_i for MeO-X04) values

lower than the CAC of Aβ$_{42}$ (90 nM), indicating that these probes detect the monomeric form of Aβ with much higher affinity. In other words, these probes cannot distinguish between monomeric and oligomeric forms of Aβ. Therefore, PyrPeg is a superior probe for the diagnosis of AD as compared to other probes mentioned above.

Docking Analysis of PyrPeg with a Aβ$_{42}$ Multimer. To visualize the molecular interactions of the Aβ$_{42}$ multimer with PyrPeg in detail, we performed a molecular docking analysis (Figures 2e and S6). Inspection of the docked pose of PyrPeg revealed that the ligand was docked deep inside the pocket formed by the Aβ$_{42}$ multimer and engaged in significant interactions with the binding-site residues (Figure 2e). 2D interaction images show the interactions of PyrPeg with the Aβ$_{42}$ multimer in detail (Figure S6). A hydrogen bond interaction, which is stronger than a van der Waals interaction, is present between the histidine 14 residue of Aβ$_{42}$ monomer B (HIS B: 14) and the oxygen (O) of polyethylene glycol. There is a π–π stacking interaction between HIS C: 14 and the first benzofuran ring of PyrPeg. The benzofuran ring also features both an amide–π interaction with GLY D: 33 and a π–alkyl interaction with ILE D: 32. The central pyrazine ring is engaged in both an amide–π stacked interaction with GLY E: 33 and a π–alkyl interaction with ILE E: 32. Nonetheless, the other benzofuran moiety takes part in an amide–π stacked interaction with ILE F: 32. These π stacked interactions are noncovalent bonds and pivotal to biological events such as protein–ligand recognition. Most of the other interactions are carbon–hydrogen and van der Waals interactions,

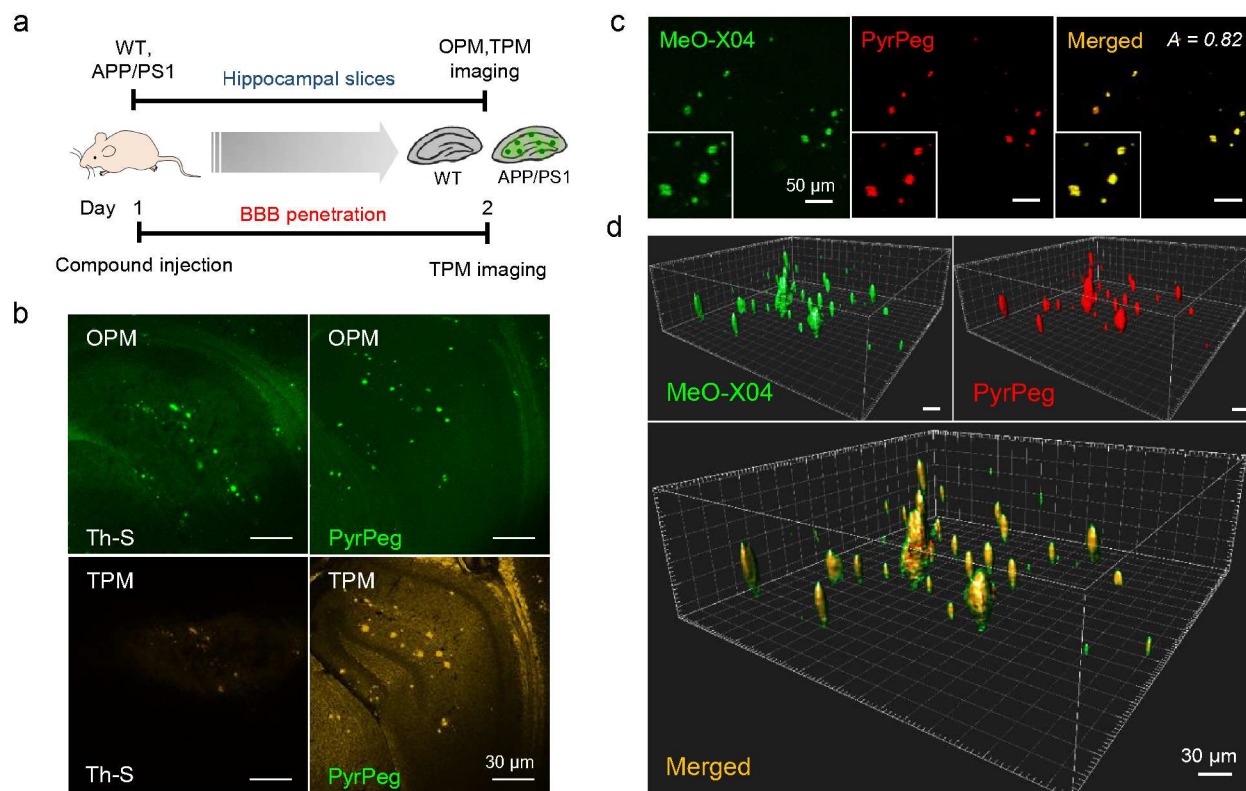suggesting that PyrPeg forms strong covalent bond interactions with Aβ oligomers.

Figure 3. Detection of neuritic plaques in APP/PS1 mice. (a) A schematic diagram of *ex vivo* and *in vivo* imaging of a tail-injected mouse. (b) OPM and TPM images of APP/PS1 mouse brain slices labeled with Th-S and PyrPeg. (c) TPM images of an APP/PS1 mouse brain slice 1 day after i.p. injection with MeO-X04 (2 mg/kg) and i.v. injection with PyrPeg (2 mg/kg) and a merged image (yellow). The images were captured at 400–500 nm (MeO-X04, green) and 530–640 nm (PyrPeg, red) upon TP excitation at 750 nm at a depth of 200 μm. (d) 3D images constructed from 200 sectional images of the MeO-X04– and PyrPeg-injected tissues at a depth of 150–300 μm with 0.75 μm intervals along the z-direction and a merged image. The merged image shows green dots around the overlapping regions. Representative images from replicate experiments (n = 3) are presented. Scale bars: 30 and 50 μm.

BBB Penetration, a Neuritic-Plaque-Tracking Ability, and Cytotoxicity. As an optimal *in vivo* brain-imaging probe, PyrPeg must meet several requirements, which include optimal lipophilicity (logP value between 2 and 4),[22,23] the ability to penetrate the BBB as estimated by the parallel artificial membrane permeability (PAMPA) assay, and low cytotoxicity. We first calculated logP and performed the PAMPA-BBB assay. The logP value was 3.51, and the PAMPA experiment yielded positive results on the prediction of BBB penetration (Table S3). Indeed, in an OPM image, the fluorescence—as measured by total area, average plaque size, percent plaque area, and the number of plaques—of PyrPeg in APPswe/PSEN1dE9 (APP/PS1) mice, which were euthanized 24 h after intravenous injection of 0–20 mg/kg PyrPeg, increased with increasing concentrations of PyrPeg (Figure S7a–e). This finding confirmed that PyrPeg could cross the BBB. Moreover, the fluorescence of PyrPeg remained in the APP/PS1 mice for 2 weeks after the injection (Figure S7f,g). This persistent fluorescence is probably due to the numerous carbon–hydrogen and π-stacking interactions of PyrPeg with Aβ oligomers, which provide a stable environment within the binding pocket formed by the Aβ multimers (Figures 2e and S6). We then examined the toxicity of PyrPeg by the 3-

(4,5-dimethylthiazol-2-yl)-2,5 diphenyltetrazolium-bromide (MTT) assay (for astrocytes) and the CCK-8 assay (for SH-SY5Y cells). We found that PyrPeg was not toxic to astrocytes at ≤0.1 μM (Figure S8a), which is the working concentration of PyrPeg (see below), and manifested only minimal cytotoxicity at concentrations up to 10 μM in SH-SY5Y cells (Figure S8b). Additionally, PyrPeg showed no apparent toxicity up to 100 mg/kg, as indicated by 100% survival rates of C57BL/6J mice that were intravenously injected 10–100 mg/kg of PyrPeg into the tail (Figure S8c). These results mean that PyrPeg is an excellent brain-imaging probe for the detection of Aβ plaques *in vivo* according to its excellent BBB penetration, persistent binding with Aβ plaques, and low cytotoxicity.

Utility of PyrPeg for TPM Imaging. To test whether PyrPeg is optimized for TP imaging, we measured the TPEF intensity of PyrPeg and compared the Φδ values of PyrPeg with those of Th-S, Aβ probe 5, and MeO-X04 (Figure 1d). PyrPeg has $\Phi\delta_{max}$ of 230 GM at 740 nm (Table 1). In sharp contrast, $\Phi\delta_{max}$ of Th-S was found to be 8 GM (Figure 1d), too low to yield bright TPM images (Figure 3b), making Th-S an inefficient TP probe compared to PyrPeg. Besides, $\Phi\delta_{max}$ of Aβ probe 5 was only 4 GM (Table S1); this is a TP probe having K_d (44.6 nM) most similar to that of PyrPeg (63.8 nM) among others according to the literature. Furthermore, 10-fold higher laser power (50 mW) than that
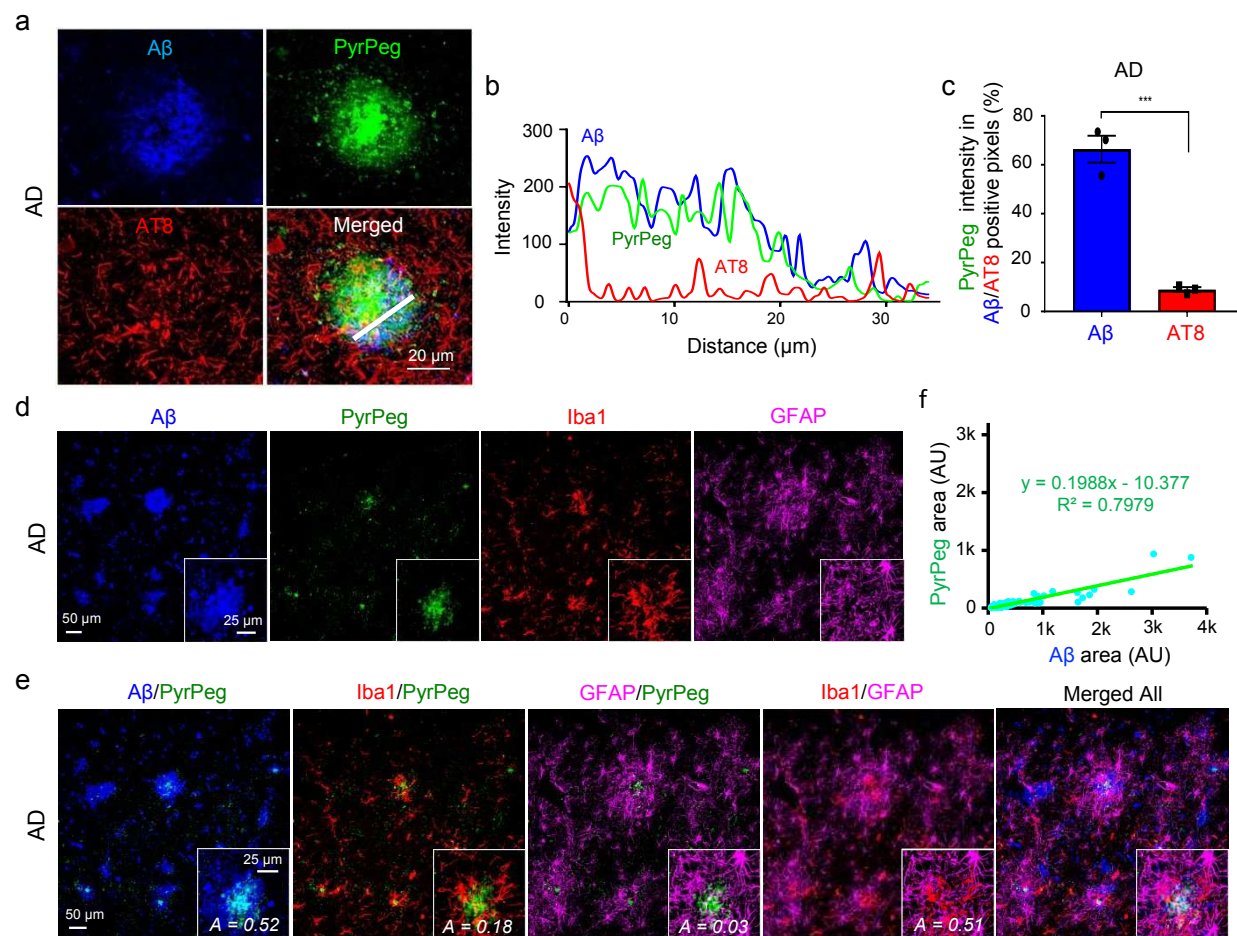
Figure 4. Detection of neuritic plaques in a human AD brain section. (a) OPM images of the normal and AD patient's brain sections costained with an anti-Aβ antibody (blue), anti-phospho-tau antibody (AT8; red), and PyrPeg (green) and a merged image. (b) Line measurement analysis along the white line in the merged image of (a). (c) Normalized PyrPeg intensities in the Aβ- and AT8-positive pixels. ***$P < 0.001$, two-tailed Student's unpaired t test. (d) OPM images of a human AD brain section stained with an anti-Aβ antibody (blue), PyrPeg (green), anti-Iba1 antibody (red), and anti-GFAP antibody (magenta). (e) Merged images. (f) A plot of PyrPeg-positive vs. Aβ-positive areas using 76 data points from three OPM images. Green dots are the experimental data, and the straight line is the linear regression line that can be represented by the empirical equation shown in the figure. Representative images from replicate experiments (n = 3) are presented. Scale bars: 20, 25, 50, and 100 μm.

employed for PyrPeg is required to obtain TPM images of Aβ plaques in the frontal cortex of a 5XFAD mouse after intraperitoneal (i.p.) injection of Aβ probe 5.[6] Such high laser power can be detrimental to the tissue.[16] On the contrary, $\Phi\delta_{max}$ of MeO-X04 was 75 GM in EtOH, i.e., 3-fold lower than that of PyrPeg. Nevertheless, it was possible to obtain TPM images of brain slices from APP/PS1 mice 1 day after i.p. injection with MeO-X04 (2 mg/kg; Figure 3). We also measured the effective TP action cross-section ($\Phi\delta_{eff}$) by comparing the TPEF intensity of Aβ peptide–treated SH-SY5Y cells labeled with 0.1 μM PyrPeg with that of Rhodamine 6G under the same imaging conditions. $\Phi\delta_{eff}$ was 1520 GM (Table 1). The local concentration of PyrPeg in the bright spot of the TPM image, which was calculated by dividing $\Phi\delta_{eff}$ by $\Phi\delta$ measured in the model solvent, was 7 μM, 70-fold higher than that in the staining medium—a result that can be attributed to the more favorable interactions between the probe and intracellular environment than those with the staining medium. To determine the optimum probe

concentration in the imaging experiments, we measured $\Phi\delta$ values in PyrPeg-stained brain slices of APP/PS1 mice. This strain is the most commonly used transgenic mouse model of AD. Given that the APP/PS1 brain slices stained with 0.1–1.0 μM PyrPeg showed almost the same TPEF intensities, we used 0.1 μM PyrPeg in all the imaging experiments (Figure S9).

Photostability is one of the key properties of a TP probe because bioimaging requires sustained stable fluorescence intensity with long excitation duration. Therefore, we measured the photostability by monitoring the fluorescence intensity during 1 h of continuous excitation. Owing to the low fluorescence of Th-S in TP imaging, we compared the one-photon fluorescence intensity of Th-S with the TPEF of MeO-X04 and PyrPeg (Figures 3b–d). We observed severe photobleaching of Th-S, whose fluorescence decreased by half after 3500 s, and during the same period, MeO-X04 showed a 13% decrease in the TPEF intensity (Figures S10g,h). By contrast, the TPEF intensity of PyrPeg remained nearly the same for 2000–3500 s

(Figure S10f), which was also observed in SH-SY5Y cells (Figure S10e). These results indicate that, unlike Th-S and MeO-X04, PyrPeg has excellent photostability.

To validate the superiority of PyrPeg over Th-S and MeO-X04 for TP imaging, we compared the fluorescence intensities of PyrPeg and Th-S in TPM and OPM images of brain slices from wild type (WT) and APP/PS1 mice (Figures 3d and S11). The WT mouse slices labeled with Th-S and PyrPeg emitted no fluorescence according to the OPM and TPM images because of the absence of Aβ plaques (Figure S11). In the OPM images, both PyrPeg and Th-S had significant fluorescence intensities in APP/PS1 mice (Figure 3b, upper panel). By contrast, in the TP images from APP/PS1 mice, only PyrPeg had high TPEF intensity, whereas Th-S showed very low TPEF intensity (Figure 3b, lower panel).

We next compared the utility of PyrPeg and MeO-X04 for TPM imaging. We prepared brain slices from APP/PS1 mice 1 day after i.p. injection with MeO-X04 (2 mg/kg) and intravenous injection with PyrPeg (2 mg/kg) and acquired 200 sectional images in a probe-labeled tissue at a depth of 150–300 μm with 0.75 μm intervals along the z-direction using the detection windows at 400–500 nm (MeO-X04, channel 1 [Ch1]) and 530–640 nm (PyrPeg, Ch2). The sectional images captured in Ch1 and Ch2 at a depth of 220 μm overlapped well, with the A value of 0.82 (Figure 3c, right). Moreover, the 3D images constructed from 200 sectional images collected in Ch1 and Ch2 overlapped well except for the green dots (MeO-X04) scattered around the overlap region (yellow dots) that can be attributed to the tangles and cerebrovascular amyloids.[24] This outcome indicates that PyrPeg is localized in the dense core region of the neuritic Aβ plaque. Therefore, among the currently available Aβ probes, PyrPeg is the most optimal probe for TPM.

***Ex Vivo* Detection of Neuritic Plaques in a Postmortem AD-Affected-Brain Section.** To test whether PyrPeg can specifically label Aβ plaques in human AD-affected-brain sections, but not in healthy brain tissue, we stained the tissues with an anti-Aβ antibody, PyrPeg, and anti–phospho-tau (S202/T205) antibody (called "AT8"; Figure 4a). The fluorescence of PyrPeg colocalized with Aβ but not with AT8 in the AD-affected brain. In sharp contrast, healthy brain tissue emitted no fluorescence (Figure S12). Moreover, the normalized PyrPeg intensity in Aβ-positive pixels was significantly higher than that in AT8-positive pixels (Figure 4c). We also conducted a line measurement analysis to examine the specific colocalization patterns of PyrPeg with Aβ and AT8 in the AD brain and in APP/PS1 mouse sections. We found strong colocalization of PyrPeg with Aβ, but not with AT8, in both human AD brain sections and APP/PS1 mice (Figures 4b and S13b). These data confirm that PyrPeg can selectively detect Aβ plaques despite the presence of tau aggregates. In addition, the PyrPeg-positive area correlated well with the Aβ-positive area on a straight line with a slope of 0.2, indicating that the former is always smaller than the latter regardless of the plaque size (Figure 4f). This outcome could be interpreted as PyrPeg's labeling the core of the Aβ

plaques, as illustrated in Figures 2a and 3d. On the contrary, the PyrPeg-positive area did not overlap with the Iba1-positive microglia or GFAP-positive astrocytes (as indicated by small A values, <0.2) but was surrounded by them, except that a few of these areas were found in the core of the plaque in AD brain sections (Figure 4e, inset). This result is in slight contrast to the finding in APP/PS1 mice, which showed a better overlap of Iba1- and PyrPeg-positive regions (A = 0.18 *vs.* 0.70) and a poorer overlap of Iba1- and GFAP-positive regions (A = 0.51 *vs.* 0.03; Figures 4e and S14). This result can be attributed to a difference in clinical stages between human AD and the mouse AD model (APP/PS1). These data suggest that PyrPeg can specifically label the core of the neuritic plaques surrounded by microglia and reactive astrocytes in samples of human AD-affected brain tissue.

***In Vivo* Detection of Neuritic Plaques in the Olfactory Bulb of APP/PS1 Mice.** We examined TPEF by *in vivo* live imaging in the olfactory bulb of APP/PS1 mice injected with PyrPeg. Because the olfactory bulb is primarily affected in AD,[25,26] its monitoring can provide an indicator of the progression of presymptomatic AD. Hence, we intravenously injected 1 mg/kg PyrPeg into WT and APP/PS1 mice on day 1 and examined the fluorescence by TP live imaging on day 2 (Figure 5b). *In vivo* TPM imaging was conducted through a well-established open-skull window on the olfactory bulb. The image shows bright fluorescence from PyrPeg in the APP/PS1 mice (Figure 5b, right) but not in the WT mice (Figure 5b, left). Thus, we propose that PyrPeg is useful for the detection of neuritic plaques as a TPM *in vivo* dye. Therefore, we conclude that PyrPeg selectively labels aggregated forms of Aβ fibrils and neuritic plaques—not tau tangles—in the AD brain, suggesting that PyrPeg may be useful for AD diagnosis.
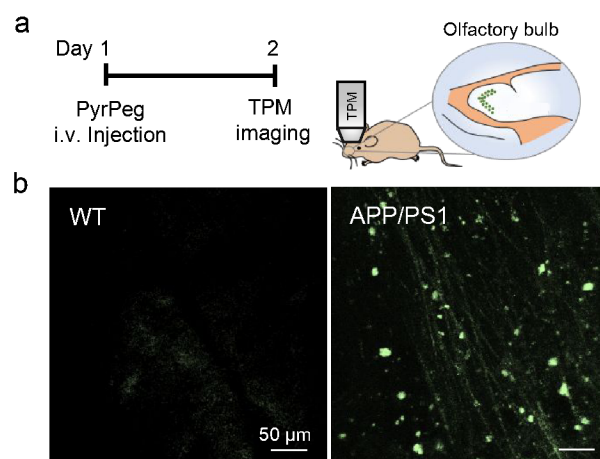

Figure 5. *In vivo* TPM images of the olfactory bulb in mice. (a) Schematic diagram of *in vivo* TPM imaging of the olfactory bulbs of a tail-injected mouse. (b) TPM images of the olfactory bulbs of WT (left) and APP/PS1 mice (right) 1 day after injection with PyrPeg (1 mg/kg). Scale bar: 50 μm.

CONCLUSION

PyrPeg is free of the drawbacks of the existing AD imaging probes for the detection of Aβ aggregates. The most crucial feature of PyrPeg is its ability to stain Aβ aggregates, especially neuritic plaques. PyrPeg should be useful for longitudinal monitoring of neuritic plaques according to its selectivity for Aβ fibrils and long-term stability, warranting the aforementioned possible clinical uses. Given that neuritic plaques are strongly associated with the pathological causes of neurodegeneration and cognitive deficits, PyrPeg will provide critical missing information concerning AD pathogenesis and may help to find new therapeutic approaches.

In summary, PyrPeg has many essential advantages for the detection of Aβ plaques via *in vivo* TP imaging and is free of the drawbacks of existing probes. In particular, PyrPeg was proven here to be superior to these existing probes in detecting neuritic plaques. We propose that the bioimaging of neuritic plaques using PyrPeg may serve as a useful diagnostic tool for AD.

METHODS

Animals. APP/PS1 mice with a B6C3 hybrid background were obtained from Jackson Laboratory (USA, stock number 004462) and maintained as hemizygotes by crossing transgenic mice with B6C3 F1 mice, which were derived from a cross between a C57BL/6J female and C3H male. This hybrid strain is commonly employed for the production of transgenic mice. Both sexes of 8- to 13-month-old transgenic mice and WT littermates were used.

Cell Culture. Primary cortical astrocytes were prepared from 1-day-old postnatal C57BL/6J mice and maintained in a culture medium, as previously reported.[27] The cultures were maintained at 37 °C in a humidified atmosphere containing 5% of CO_2. Three days later, the cells were vigorously washed by repeated pipetting with the culture medium, and the medium was replaced to remove debris and other floating cell types. SH-SY5Y cells were all obtained from the American Type Culture Collection (Rockville, MD) and cultured according to their specifications. The SH-SY5Y cells were cultured in the Minimum Essential Medium (MEM, WelGene). The medium was supplemented with 10% of fetal bovine serum (FBS, WelGene), with penicillin (100 U/mL), and streptomycin (100 µg/mL). Two days before imaging, the cells were detached and placed on glass-bottomed dishes (MatTek). For labeling, the growth medium was replaced with MEM without FBS.

Aβ42, α-syn, and Tau protein. Aβ42 peptide (H2N-DAEFRHDSGYEVHHQKLVFFAEDVGSNKGAIIGLMVGGVVIA-COOH) was prepared as previously described (Figure S15).[20] Recombinant human α-synuclein (AnaSpec, AS-55555), and Tau 441 (AnaSpec, AS-55556) proteins were commercially available and used as received.

Synthesis of PyrPeg. This procedure is described in the Supporting Information.

Solubility. The solubility of PyrPeg in PBS was determined by the absorbance method because of the negligible fluorescence in water.[28] Briefly, small increments of PyrPeg in dimethyl sulfoxide (DMSO, 10^{-3} M) were added into a cuvette containing 3.0 mL of PBS by means of a micropipette while the DMSO concentration in the cuvettes was maintained at 0.2%. The absorbance of the solution was measured and plotted against the probe concentration. The maximum concentration in the linear region of the plot was taken as the solubility.

Lipophilicity (LogP). This property of PyrPeg was calculated in the ACDLab-ACD LogP software.[29]

PAMPA-BBB Assay. These assays were performed using the PAMPA Explorer Kit (pION Inc.) according to the manufacturer's instructions. Stock solutions of a sample were prepared in DMSO (10 mM). The stock solution was diluted with Prisma HT buffer (pH 7.4) to a final concentration of 50 µM. After that, 200 µM of the resulting stock solution was added into each well of donor plates (n = 3). The polyvinylidene difluoride (0.45 µm) filter membrane on the acceptor plate was coated with 5 µL of the BBB-1 lipid. Each well of the acceptor plate was filled with 200 µL of brain sink buffer. The acceptor plate was placed on the donor plate to form a sandwich; the sandwich was incubated at 37 °C for 4 h without stirring. UV–Vis spectra of the solutions for reference, acceptor, and donor plates were registered on a plate reader (Infinite 200 PRO, Tecan). Effective permeability (Pe) for the sample was calculated using the PAMPA Explorer software v.3.5 (pION). Theophylline served as a negative control, and lidocaine and progesterone were used as positive controls for this assay.

Spectroscopic Measurements. Absorption and fluorescence spectra were recorded on an Agilent 8453 diode array UV–Vis spectrophotometer and a HITACHI F-7000 fluorescence spectrophotometer using a 1 cm standard quartz cell, respectively. The fluorescence quantum yield (Φ) was determined by using Coumarin 307 as the reference, as reported elsewhere.[30]

Cytotoxicity. The cytotoxicity of PyrPeg to SH-SY5Y cells and astrocytes was measured by means of a Cell Counting Kit-8 (CCK-8 kit, Dojindo, Japan) and MTT Assay Kit (Abcam, ab211091) following the manufacturer's protocols.

Photostability. This property of PyrPeg was determined by monitoring TPEF intensity in SH-SY5Y neuronal cells and *ex vivo* APP/PS1 brain slices labeled with PyrPeg, Th-S, and MeO-X04, as previously reported.[15]

Measurements of Φδ. This characteristic of PyrPeg was determined by a fluorescence method, as described previously.[31]

Measurement of Φδ_eff. This parameter was determined as reported elsewhere.[30] Briefly, TPEF intensities of PyrPeg-labeled cells and 5.0 µM Rhodamine 6G in MeOH in delta T-dishes were measured using the TPM setup. Φδ_eff was calculated via the formula $\Phi\delta_{eff} = \Phi_r\delta_r(I_p/I_r)$, where I_p and I_r are the TPEF intensities from the probe-labeled cells and 5.0 µM Rhodamine 6G in MeOH in delta T-dishes in the TPM setup, respectively.

1
2
3
4
5
6
7
8
9
10
11
12
13
14
15
16
17
18
19
20
21
22
23
24
25
26
27
28
29
30
31
32
33
34
35
36
37
38
39
40
41
42
43
44
45
46
47
48
49
50
51
52
53
54
55
56
57
58
59
60

SPR Analysis. This analysis was performed using a BIAcore T200 system equipped with CM5 sensor chips (GE Healthcare). The monomeric or oligomeric Aβ was immobilized on a chip to attain a density of 2900–3200 response units (RU) by amine coupling protocols.[32] The stock solution of PyrPeg in PBS-P (GE Healthcare, final DMSO solution) was serially diluted to prepare a series of PyrPeg solutions with different concentrations. The solutions were injected over the conjugated chip at a flow rate of 30 μL/min (contact time: 120 s, dissociation time: 300 s), and the regeneration step was performed at a flow rate of 30 μL/min (contact time: 30 s, stabilization time: 10 s). The K_d values were calculated in the BIAcore evaluation software (GE Healthcare) after the standard solvent correction process.

Antibodies. The primary antibodies used for immunostaining were as follows: chicken anti-GFAP (1:500, Millipore, ab5541), mouse anti-α-synuclein (1:200, Abcam, ab1903), rabbit anti-tau (1:200, Abcam, ab81268), rabbit anti-amyloid beta (1:500, Abcam, ab2539), and mouse anti-iba1 (1:200, Millipore, MAB3402). The following fluorescent secondary antibodies were utilized: an Alexa Fluor 405–conjugated goat anti-rabbit IgG antibody, Alexa Fluor 594–conjugated goat anti-mouse IgG antibody, Alexa Fluor 594–conjugated goat anti-rabbit IgG antibody, and Alexa Fluor 647–conjugated donkey anti-chicken IgY antibody. Secondary antibodies were purchased from Invitrogen or Jackson ImmunoResearch and used at 1:200 dilution.

TPM Imaging. TPM images of SH-SY5Y cells, AD model mouse tissue, and human postmortem AD-affected-brain sections labeled with PyrPeg were obtained over the 450–650 nm range by multiphoton microscopy, as previously described.[33] To determine the optimum probe concentration, we incubated the AD model mouse tissues with 0.1–1.0 μM PyrPeg for 30 min, and the TPM images were compared. TPM images of PyrPeg-labeled cells and tissues were obtained by means of spectral confocal and multiphoton microscopes (Leica TCS SP2; Leica Camera, Solms, Germany), using the 100× oil objective with a numerical aperture of 1.30 and a 10× dry objective with a numerical aperture of 0.30. The excitation was implemented using a mode-locked titanium-sapphire laser (Chameleon, 90 MHz, 200 fs; Coherent Inc., Santa Clara, CA, USA) set to 750 nm and to an output power of 1305 mW, which corresponded to 4×10^9 mW/cm² (100×) at the focal plane. Images were captured by PMTs in an 8-bit unsigned 512 × 512 pixel format at a scan speed of 400 Hz. *In vivo* optical imaging was performed by using a modified MOM two-photon laser-scanning microscope (Sutter Instruments, Novato, CA, USA) based on a mode-locked Ti-sapphire laser (Chameleon Vision S, Coherent, Santa Clara, CA, USA) and scanning with an XY galvanometric scanning set (Cambridge Technologies, Bedford, MA, USA). The microscope was equipped with a water immersion objective, Nikon LWD 16X, 0.8 N.A. (Nikon Instruments, Melville, NY, USA). PyrPeg was excited at 920 nm. Emitted light that was filtered through a 510/84 bandpass filter

(Semrock, Rochester, NY, USA) was detected with a GaAsP photomultiplier (Hamamatsu H10770).

Molecular Docking. The structure of human Aβ$_{42}$ determined by NMR spectroscopy was retrieved from the Protein Data Bank (PDB ID: 2MXU). The downloaded structure was optimized at the default level using the protein preparation wizard in Schrödinger Maestro (Schrödinger Release 2017-4: LLC, New York, NY 2017). The structures of PyrPeg were sketched using ChemDraw Professional 16 and imported into the Maestro LigPrep module at the default settings. Because the exact binding site on Aβ$_{42}$ for these ligands is not known, a grid covering the full structure of the Aβ$_{42}$ multimers was assigned for the docking analysis. In this way, the ligands could find the most favorable binding sites in the Aβ$_{42}$ multimers. The docking analysis was conducted by means of the Glide module with the standard precision (SP) docking algorithm. Fifty docking solutions were generated for each ligand, and these were ranked according to the most negative glide docking score. A more negative glide docking score implies tighter binding and vice versa. Figures were rendered using Discovery Studio Client 2018 (Dassault Systèmes BIOVIA, Discovery Studio Modeling Environment, Release 2018, San Diego: Dassault Systèmes, 2018) and PyMOL 2.1.0.

Preparation of the Animal Model. Mice were tail vein–injected with 100 μL of a PyrPeg solution via a 29-gauge insulin needle. To study the dose-dependent effect of PyrPeg on labeling, we injected 1, 3, 10, or 20 mg/kg PyrPeg into APP/PS1 mice and euthanized the mice after 24 h. To study the time-dependent effect of PyrPeg on labeling, we injected 1 mg/kg PyrPeg into the APP/PS1 mice and euthanized them from 1 day to 2 weeks after injection. In the MeO-X04 experiment, mice were i.p. injected with 100 μL of 2 mg/kg MeO-X04 (3.3% volume of a 10 mg/mL stock solution in DMSO, 6.7% volume of Cremophore EL [Sigma Aldrich, St. Louis, MO, USA]) in 90% volume of PBS. The systemic injection was carried out 24 h before imaging.[8]

Staining of Human AD-Affected Tissue. Neuropathological processing of control and AD human brain samples followed the procedures previously established by the BUADC. Next of kin provided informed consent for participation and brain donation. The study protocol was reviewed by the Boston University School of Medicine Institutional Review Board and was approved as exempt because the study deals only with postmortem collected tissue and consequently does not involve live human subjects. The study was performed in accordance with the principles of human subject protection in the Declaration of Helsinki. Detailed information concerning the brain tissue samples is given in Table S1. No unexpected or unusually high safety hazards were encountered during this study.

Confocal Microscopy of Human Brain Tissue. Paraffin-embedded human normal and AD-affected brain sections were deparaffinized and dehydrated through a series of treatments with ethanol. The tissue slides were incubated for 1 h in a blocking solution [5% bovine serum albumin

(BSA) and 0.3% Triton X-100 in 0.02 M Tris-buffered saline (TBS)] and then incubated with an anti–phospho-tau (S202/T205) antibody (phospho-PHF-tau pSer202 + pThr205 antibody, AT8; Thermo Fisher Scientific) at 4 °C overnight. After washing in TBS twice, the sections were incubated for 1 h with a fluorescently labeled secondary antibody (an Alexa Fluor 488–conjugated goat antibody to rabbit IgG; Abcam). The slides were washed with TBS three times. Next, the tissue slides were treated with PyrPeg (0.1 μM) for 30 min and washed with TBS three times. The fluorescence signals were visualized using an A1 Nikon confocal microscope. The Aβ fluorescence signal was also detected with a mouse monoclonal anti-Aβ antibody (cat. No. SIG-39320, BioLegend) (1:200 dilution).

Animal Surgery and Preparation. Mice (10-months old) were anesthetized with ketamine/xylazine (0.1/0.01 mg/g of body weight). Anesthesia was monitored by toe pinch, whisker movement, and respiration rate and was maintained by additional injections of ketamine/xylazine (0.05/0.005 mg/g of body weight). Animal care and experiments were carried out in accordance with institutional guidelines of KIST. Mice were kept at 37 °C using a homeothermic heating blanket and were regularly injected with Ringer's solution (140 mM NaCl, 5 mM KCl, 1 mM $MgCl_2$, 2 mM $CaCl_2$, 10 mM 4-(2-hydroxyethyl)-1-piperazineethanesulfonate [HEPES], and 8.9 mM D-dextrose) for hydration. Bupivacaine (0.05 mL of a 0.5% solution) was injected into the incisions. A longitudinal incision was made from behind the ear to posterior to the nose, and the skin was removed to expose the skull. A custom-made headpost was then attached on the cleaned skull with cyanoacrylic glue and dental cement (Vertex Orthoplast, Vertex-Dental, Zeist, Holland). The skull over the olfactory bulb was thinned with a dental drill, and craniotomy with a 1.5–2.5 mm diameter was performed by removing the thinned bone. Finally, 2% agarose in Ringer's solution and a glass window were placed over the olfactory bulb.

ASSOCIATED CONTENT

Supporting Information
The Supporting Information is available free of charge on the ACS Publications website at DOI:

Experimental details on the synthesis of compounds, spectroscopic characterization of the compounds, photostability, viability of SH-SY5Y cells in the presence of PyrPeg probes, TPM images of SH-SY5Y cells and astrocytes labeled with PyrPeg, immunostaining of PyrPeg in APP/PS1 mice, TPM images of a brain tissue colabeled with PyrPeg and MeO-X04, PAMPA-BBB data, ^1H and ^{13}C NMR spectra, and high-resolution mass spectra (PDF)

AUTHOR INFORMATION

Corresponding Authors
*E-mail: chobr@korea.ac.kr
*E-mail: cjl@ibs.re.kr

Author Contributions

◇ J.-W.C. and Y. H.J. contributed equally to this work.

Notes
The authors declare no competing financial interest.

REFERENCES

(1) Jack, C. R., Jr.; Bennett, D. A.; Blennow, K.; Carrillo, M. C.; Dunn, B.; Haeberlein, S. B.; Holtzman, D. M.; Jagust, W.; Jessen, F.; Karlawish, J.; Liu, E.; Molinuevo, J. L.; Montine, T.; Phelps, C.; Rankin, K. P.; Rowe, C. C.; Scheltens, P.; Siemers, E.; Snyder, H. M.; Sperling, R.; Contributors. NIA-AA Research Framework: Toward a biological definition of Alzheimer's disease. *Alzheimers Dement.* **2018**, *14*, 535–562.

(2) Arnold, S. E.; Hyman, B. T.; Flory, J.; Damasio, A. R.; Van Hoesen, G. W., The topographical and neuroanatomical distribution of neurofibrillary tangles and neuritic plaques in the cerebral cortex of patients with Alzheimer's disease. *Cereb Cortex* **1991**, *1*, 103-116.

(3) Khachaturian, Z. S., Diagnosis of Alzheimer's disease. *Arch Neurol* **1985**, *42*, 1097-1105.

(4) Masliah, E.; Mallory, M.; Hansen, L.; DeTeresa, R.; Alford, M.; Terry, R. Synaptic and neuritic alterations during the progression of Alzheimer's disease. *Neurosci Lett* **1994**, *174*, 67-72.

(5) Linke, R. P. Highly sensitive diagnosis of amyloid and various amyloid syndromes using Congo red fluorescence. *Virchows Arch* **2000**, *436*, 439–448.

(6) Kim, D.; Moon, H.; Baik, S. H.; Singha, S.; Jun, Y. W.; Wang, T.; Kim, K. H.; Park, B. S.; Jung, J.; Mook-Jung, I.; Ahn, K. H. Two-photon absorbing dyes with minimal autofluorescence in tissue imaging: Application to in vivo imaging of amyloid-beta plaques with a negligible background signal. *J. Am. Chem. Soc.* **2015**, *137*, 6781–6789.

(7) Tong, H. J.; Lou, K. Y.; Wang, W. Near-infrared fluorescent probes for imaging of amyloid plaques in Alzheimer's disease. *Acta Pharm. Sin. B* **2015**, *5*, 25–33.

(8) Klunk, W. E.; Bacskai, B. J.; Mathis, C. A.; Kajdasz, S. T.; McLellan, M. E.; Frosch, M. P.; Debnath, M. L.; Holt, D. P.; Wang, Y.; Hyman, B. T. Imaging Abeta plaques in living transgenic mice with multiphoton microscopy and methoxy-X04, a systemically administered Congo red derivative. *J. Neuropathol. Exp. Neurol.* **2002**, *61*, 797–805.

(9) Heo, C. H.; Kim, K. H.; Kim, H. J.; Baik, S. H.; Song, H.; Kim, Y. S.; Lee, J.; Mook-jung, I.; Kim, H. M. A two-photon fluorescent probe for amyloid-beta plaques in living mice. *Chem. Commun. (Camb.)* **2013**, *49*, 1303–1305.

(10) Heo, C. H.; Sarkar, A. R.; Baik, S. H.; Jung, T. S.; Kim, J. J.; Kang, H.; Mook-Jung, I.; Kim, H. M. A quadrupolar two-photon fluorescent probe for *in vivo* imaging of amyloid-beta plaques. *Chem. Sci.* **2016**, *7*, 4600–4606.

(11) Nilsson, K. P. Small organic probes as amyloid specific ligands--past and recent molecular scaffolds. *FEBS Lett.* **2009**, *583*, 2593–2599.

(12) Novo, M.; Freire, S.; Al-Soufi, W. Critical aggregation concentration for the formation of early Amyloid-β (1–42) oligomers. *Sci. Rep.* **2018**. 8, 1783.

(13) Chun, H. J.; Kim, E. S.; Cho, B. R. Scope and limitation of label-free multiphoton microscopy and probe-labeled two-photon microscopy for the endomicroscopic diagnosis. *Scanning* **2014**, *36*, 462–464.

(14) Choi, J. W.; Hong, S. T.; Kang, D. E.; Paik, K. C.; Han, M. S.; Lim, C. S.; Cho, B. R., Two-photon tracer for human epidermal growth factor receptor-2: Detection of breast cancer in a live tissue. *Anal. Chem.* **2016**, *88*, 9412–9418.

(15) Lim, C. S.; Hong, S. T.; Ryu, S. S.; Kang, D. E.; Cho, B. R. Two-photon probes for lysosomes and mitochondria: Simultaneous detection of lysosomes and mitochondria in live tissues by dual-color two-photon microscopy imaging. *Chem. Asian. J.* **2015**, *10*, 2240–2249.

(16) Hofslokken, N. U.; Skattebol, L. Convenient method for the ortho-formylation of phenols. *Acta Chem. Scand.* **1999**, *53*, 258–262.

(17) Reichardt, C. Solvatochromic dyes as solvent polarity indicators. *Chem. Rev.* **1994**, *94*, 2319–2358.

(18) Choi, J. W.; Hong, S. T.; Kim, M. S.; Paik, K. C.; Han, M. S.; Cho, B. R. Two-photon probes for golgi apparatus: Detection of Golgi apparatus in live tissue by two-photon microscopy. *Anal. Chem.* **2019**, *91*, 6669–6674.

(19) Cui, M.; Ono, M.; Watanabe, H.; Kimura, H.; Liu, B.; Saji, H. Smart near-infrared fluorescence probes with donor-acceptor structure for *in vivo* detection of beta-amyloid deposits. *J. Am. Chem. Soc.* **2014**, *136*, 3388–3394.

(20) Kim, Y. S.; Moss, J. A.; Janda, K. D., Biological tuning of synthetic tactics in solid-phase synthesis: application to A beta(1-42). *J. Org. Chem.* **2004**, *69* (22), 7776-7778.

(21) Adler, J.; Parmryd, I. Quantifying colocalization by correlation: The Pearson correlation coefficient is superior to the Mander's overlap coefficient. *Cytom. Part A* **2010**, *77a*, 733–742.

(22) Vraka, C.; Nics, L.; Wagner, K. H.; Hacker, M.; Wadsak, W.; Mitterhauser, M. LogP, a yesterday's value? *Nucl. Med. Biol.* **2017**, *50*, 1–10.

(23) Hitchcock, S. A.; Pennington, L. D. Structure-brain exposure relationships. *J. Med. Chem.* **2006**, *49*, 7559–7583.

(24) Calvo-Rodriguez, M.; Hou, S. S.; Snyder, A. C.; Dujardin, S.; Shirani, H.; Nilsson, K. P. R.; Bacskai, B. J. In vivo detection of tau fibrils and amyloid beta aggregates with luminescent conjugated oligothiophenes and multiphoton microscopy. *Acta Neuropathol. Com.* **2019**, *7*, 1–10.

(25) Kovacs, T. Mechanisms of olfactory dysfunction in aging and neurodegenerative disorders. *Ageing Res. Rev.* **2004**, *3*, 215–232.

(26) Warner, M. D.; Peabody, C. A.; Flattery, J. J.; Tinklenberg, J. R. Olfactory deficits and Alzheimer's disease. *Biol. Psychiatry* **1986**, *21*, 116–118.

(27) Hwang, E. M.; Kim, E.; Yarishkin, O.; Woo, D. H.; Han, K. S.; Park, N.; Bae, Y.; Woo, J.; Kim, D.; Park, M.; Lee, C. J.; Park, J. Y. A disulphide-linked heterodimer of TWIK-1 and TREK-1 mediates passive conductance in astrocytes. *Nat. Commun.* **2014**, *5*, 15.

(28) Kim, H. M.; Choo, H. J.; Jung, S. Y.; Ko, Y. G.; Park, W. H.; Jeon, S. J.; Kim, C. H.; Joo, T.; Cho, B. R. A two-photon fluorescent probe for lipid raft imaging: C-laurdan. *Chembiochem.* **2007**, *8*, 553–559.

(29) Mannhold, R.; Poda, G. I.; Ostermann, C.; Tetko, I. V. Calculation of molecular lipophilicity: State-of-the-art and comparison of log P methods on more than 96,000 compounds. *J. Pharm. Sci.* **2009**, *98*, 861–893.

(30) Demas, J. N.; Crosby, G. A. Measurement of photoluminescence quantum yields - review. *J. Phys. Chem.-U.S.* **1971**, *75*, 991–1024.

(31) Lee, S. K.; Yang, W. J.; Choi, J. J.; Kim, C. H.; Jeon, S. J.; Cho, B. R. 2,6-Bis[4-(p-dihexylaminostyryl)styryl]anthracene derivatives with large two-photon cross sections. *Org. Lett.* **2005**, *7*, 323–326.

(32) Ultsch, M.; Li, B.; Maurer, T.; Mathieu, M.; Adolfsson, O.; Muhs, A.; Pfeifer, A.; Pihlgren, M.; Bainbridge, T. W.; Reichelt, M.; Ernst, J. A.; Eigenbrot, C.; Fuh, G.; Atwal, J. K.; Watts, R. J.; Wang, W. Structure of crenezumab complex with Abeta shows loss of beta-hairpin. *Sci. Rep.* **2016**, *6*, 39374.

(33) Otterstedt, J.-E. A. Photostability and molecular structure. *J. Chem. Phys.* **1973**, *58*, 5716–5725.

Table of Contents